

RP

ACOUSTIC RIDGE WAVEGUIDE TECHNOLOGY

Robert S. Wagers

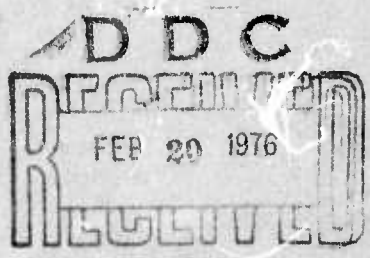
Texas Instruments Incorporated

January 1976

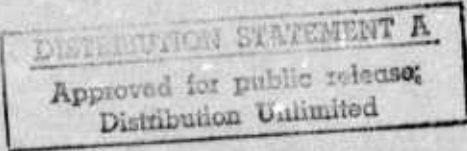
Semiannual Technical Report

30 June 1975 - 31 December 1975

Sponsored by
Advanced Research Projects Agency
ARPA Order No. 2827



The views and conclusions contained in this document are those of the authors and should not be interpreted as necessarily representing the official policies, either expressed or implied, of the Advanced Research Projects Agency or the U. S. Government.



**BEST
AVAILABLE COPY**

14
Report No.
TI-08-76-05

⑥

ACOUSTIC RIDGE WAVEGUIDE TECHNOLOGY

Contract No.

15 N00014-75-C-0317, ✓ ARPA Order - 2827

⑩

Robert S. Wagers

Texas Instruments Incorporated

11

Jan 1976

12 36 p.

⑨

Semiannual Technical Report

30 Jun 1975 - 31 Dec 1975

Sponsored by

Advanced Research Projects Agency

ARPA Order No. 2827

ARPA Order Number: 2827

Program Code Number: 5D10

Name of Contractor: Texas Instruments Incorporated
Central Research Laboratories
P. O. Box 5936
Dallas, Texas 75222

Effective Date of Contract: 6 January 1975

Contract Expiration Date: 30 June 1976

Amount of Contract: \$136,219

Contract Number: N00014-75-C-0317

Principal Investigator and Phone No.: Robert S. Wagers
(214) 238-5238

Scientific Officer: Director, Electronic and Solid
State Sciences Program
Physical Sciences Division
Office of Naval Research
800 N. Quincy Street
Arlington, Virginia 22217

Short Title of Work: Acoustic Waveguides

403 833 ✓

mt A

TECHNICAL REPORT SUMMARY

This report presents results obtained during the second six months of development of acoustic waveguides. A primary motivation for developing acoustic waveguides is to take advantage of the potential size reduction over current surface acoustic wave technology. Waveguide components represent the next step in microminiaturization of acoustic signal processing devices. Devices that may be developed include directional couplers, ring resonators, and serial memory. In addition, because of the high degree of spatial confinement of the acoustic energy, nonlinear and acousto-optic interactions become possible.

The technical problems associated with this research are threefold:
(1) development of suitable etching processes for waveguide formation,
(2) development of fine geometry stencils for transducer fabrication, and
(3) development of transducer weighting characteristics for bandpass shaping.

• Waveguide Formation

The etching process for α -quartz reported in the previous semiannual report has proved to be unsatisfactory when larger waveguide dimensions (> 0.001 inch) are required. In this process the substrates are masked off with sputtered films of chromium and gold and then etched in boiling hydrofluoric acid. We find, however, that erosion of the chromium-quartz interface occurs at a sufficiently fast and uncontrollable rate to prevent fabrication of large-dimension waveguides. In addition, the long etch times employed have revealed crystal defects in the quartz substrates. These defects appear to be cylindrical voids that originate at the seed of the boule and are maintained during crystal growth. Consequently, wafers sliced from the boule have these voids piercing them. Because the diameters of the voids are quite small, etch times of one to three hours are required to reveal them. Small waveguides (< 0.001 inch), which can be etched in quartz, require such small wavelengths and transducer geometries that their use is not feasible.

Most of this six-month period has been devoted to examining the use of lithium niobate. This material has been even more difficult to work with than quartz. A number of crystal defects have been observed and correlated to waveguide irregularities. It appears that waveguide formation on lithium niobate will not be possible without substantial improvements in crystal growth techniques.

- Transducer Fabrication

No further work was performed on stencil fabrication due to the major difficulties encountered in waveguide etching.

- Transducer Weighting Analysis

Work in this area will commence on 1 January 1976. Transducer coupling as a function of electrode geometry will be determined analytically, and experimental confirmation will be carried out on mechanically lapped waveguides.

No special equipment has been purchased or developed on this contract.

TABLE OF CONTENTS

<u>SECTION</u>		<u>PAGE</u>
I	INTRODUCTION	1
	A. Objectives	1
	B. Approach to Waveguide Development	1
	1. Waveguide Fabrication	1
	2. Transducer Fabrication	3
II	ETCHING STUDIES	4
	A. Introduction	4
	B. Etching of LiNbO ₃	4
	1. Crystal Axes Polarity of LiNbO ₃ Plates . .	4
	2. LiNbO ₃ Etch Plane	11
	3. LiNbO ₃ Waveguide Results	11
	C. Etching of α -Quartz	24
	1. α -Quartz Crystal Defects	24
	2. Other Etchants and Etch Masks For Quartz .	25
	D. Conclusion	27
III	FUTURE WORK	29

LIST OF ILLUSTRATIONS

<u>FIGURE</u>		<u>PAGE</u>
1	Acoustic Waveguides on a Piezoelectric Wafer.	2
2	Y-Surfaces of a LiNbO ₃ Wafer at ~ 500X.	6
3	Y-Surfaces of a LiNbO ₃ Wafer After Etching for about Two Hours in Boiling Concentrated HF.	7
4	Z-Surfaces of LiNbO ₃ After Etching in Boiling Concentrated HF	9
5	Scanning Electron Microscope Photographs of the Surfaces Shown and Described in Figure 4.	10
6	Schematic-Representation of LiNbO ₃ Waveguide Showing Both Rectangular and Hexagonal Axes	12
7	Etched LiNbO ₃ Waveguides.	13
8	Two Etched LiNbO ₃ Waveguides.	14
9	View at 100X Into the Y-Surface of Etched LiNbO ₃ Waveguides.	16
10	Etch Pits on the Side Wall of LiNbO ₃ Waveguides, ~ 100X.	17
11	Polishing Damage in a Field of Etched LiNbO ₃ Waveguides.	18
12	Etched LiNbO ₃ Waveguides Showing Characteristic Indentations of Apex Line	20
13	Correlation of Apex Defects With Y-Surface Line Structure	21
14	Y-Surface of LiNbO ₃ Wafer	22
15	Y-Surface of LiNbO ₃ Wafer	23
16	Waveguides on ST-Cut Quartz	26
17	Waveguides on ST-Cut Quartz	27

SECTION I

INTRODUCTION

This report presents results obtained during the second six months of development of acoustic waveguides. Section I outlines the motivation for the work and the objectives being pursued. Section II describes results obtained by etching waveguides in lithium niobate (LiNbO_3) and α -quartz. Plans for future work are discussed in Section III.

A. Objectives

A primary motivation for developing acoustic waveguides is to take advantage of the potential size reduction from current surface acoustic wave (SAW) technology. In addition, because of the high degree of spatial confinement of the acoustic energy, nonlinear and acousto-optic interactions become possible. Devices that may be developed include directional couplers, ring resonators, and serial memories.

B Approach to Waveguide Development

The basic configuration under development is shown in Figure 1. This configuration was chosen over other alternatives for two principal reasons: (1) the fundamental mode of the ideal structure is dispersionless; and (2) when the structure is fabricated on a wafer as shown, the flexure and electric potential of the guide are compatible with transducer fabrication in the plane of the wafer's top surface. Development of a delay line with the configuration of Figure 1 breaks down into two major divisions, fabrication of the waveguide and fabrication of the transducers.

1. Waveguide Fabrication

Orientation-dependent etching (ODE) of crystals has been demonstrated in many materials. Notably, silicon exhibits preferential etching, and a vast

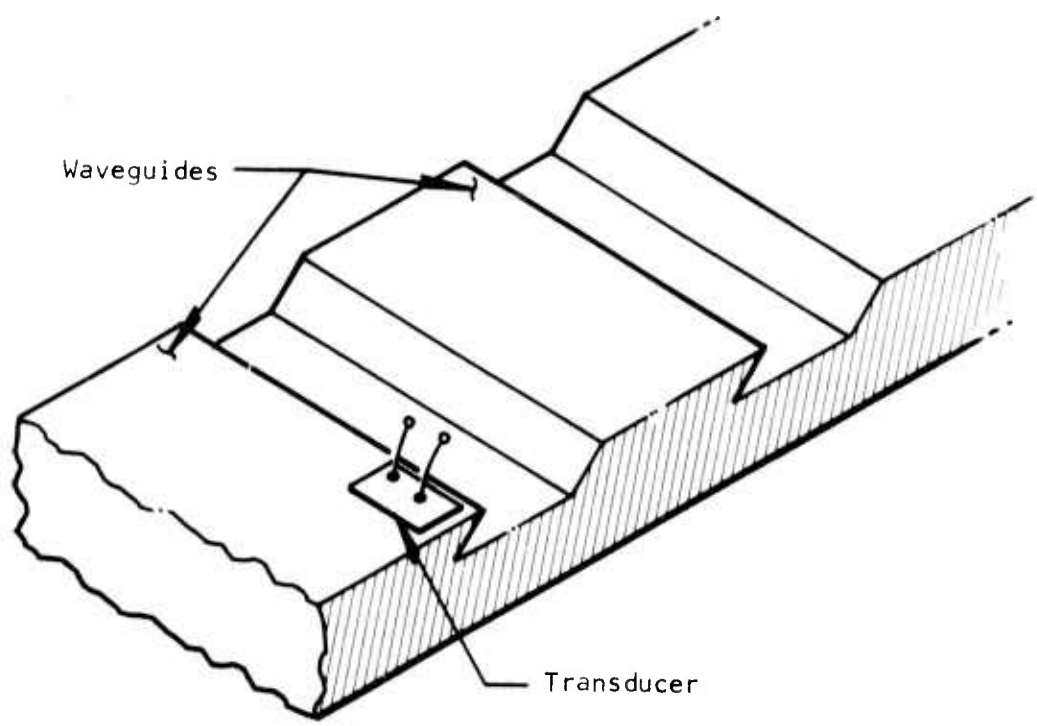


Figure 1 Acoustic Waveguides on a Piezoelectric Wafer.
The overhanging wedge-shaped structures confine
and guide the wave. Transducers are fabricated
on the face of the waveguide that is coplanar
with the top surface of the wafer.

body of literature has been produced dealing with ODE of silicon. Unfortunately, silicon is not piezoelectric, and while waveguides may be easily formed¹ in the material, transduction is an exceedingly difficult problem.

Quartz and LiNbO₃ also permit preferential etching. While no body of literature on ODE of these two materials exists, Texas Instruments, through the work of Dr. D. F. Weirauch,² has developed considerable expertise during the past year in etching device geometries in quartz and LiNbO₃. It is this ODE capability that enables us to consider the configuration of Figure 1. Our current work on ODE of LiNbO₃ and quartz is discussed in Section II.

2. Transducer Fabrication

Optimal transducer design includes not only defining a process that produces coupling metallizations on the waveguides, but also takes into account spurious mode discrimination and fundamental mode impedance matching considerations. Some work along these lines was carried out during the first six months of this investigation and was described in the first semiannual report. During the current reporting period, no additional work on transducer fabrication and impedance characterization was performed.

-
1. R. C. Rosenfeld and K. E. Bean, "Fabrication of Topographical Ridge Guides on Silicon for VHF Operation," Proc. IEEE Ultrasonics Symposium, Boston, Mass., pp. 186-189 (October 1972).
 2. D. F. Weirauch, "The Correlation of the Anisotropic Etching of Single Crystal Silicon Spheres and Wafers," J. Appl. Phys. 46, 4, 1478-1483 (April 1975).

SECTION II

ETCHING STUDIES

A. Introduction

Waveguide fabrication in LiNbO_3 and α -quartz is carried out by etching the materials in boiling concentrated hydrofluoric acid. Wafers of the materials are carefully polished on one surface and then coated with sputtered chrome and gold. Etch windows that define the waveguide apex are opened in the protective metals to expose the crystal between waveguides. Etching is then carried out in a large volume of boiling HF without mechanical agitation. Etch rates are about 40 $\mu\text{m}/\text{hour}$ and 6 $\mu\text{m}/\text{hour}$ on ST-cut quartz and +Y-cut LiNbO_3 , respectively.

Currently, two major difficulties are limiting success in the fabrication of the waveguides. One problem is that the protective metals do not adhere sufficiently well to the substrates and lift off during the etching process. This problem is considerably worse for quartz than for LiNbO_3 . The second major problem is crystal defects which etch differently from the major lattice. This problem has been worse for LiNbO_3 than for quartz. It has been only recently, as we have attempted to make larger waveguides (~ 0.003 inch), that the problem in quartz was recognized. Because of the considerable difficulties presented by the defects in LiNbO_3 , we have devoted a major portion of the last six months to examination of the crystal defects seen in this material.

B. Etching of LiNbO_3

1. Crystal Axes Polarity of LiNbO_3 Plates

Before etching waveguides in LiNbO_3 plates can be attempted, the orientation of the crystal axes must be determined. We have found that X-directed waveguides can be etched only on the +Y surface of Y-cut wafers and that those waveguides will be oriented with the apexes pointing toward the -Z direction. Consequently, the +Y surface must be identified for wafer polishing

and the -Z direction located for photomask orientation. These surfaces can be readily identified by using hydrofluoric acid as an etchant, since they manifest distinctly different appearances after etching.

Y-axis polarity of Y-cut LiNbO₃ wafers can usually be determined from the sawed wafer before etching. On the basis of observations made on Y-cut wafers obtained from several different saws, two different vendors, and three different growth directions, the following generalizations have been found to hold.

+Y-Face

This face has a "flowed" appearance and seems to show saw marks. It has a higher sheen, and the sheen is streaked. At 200X one can see what appears to be regular periodic scratches covered by a thin layer of LiNbO₃ crumbs. This face becomes negative when Y-axis compression is applied.

-Y-Face

This face appears dull, matte, and uniform. At 200X it appears to have scratches also, but it is covered by a thick layer of large LiNbO₃ crumbs. This face becomes positive when Y-axis compression is applied.

Comparative photographs at ~ 500X of the as-sawed Y-faces are shown in Figure 2. The faces have quite different appearances and are easily distinguished. Figure 3 shows the Y-faces at ~ 500X after etching for about two hours in boiling concentrated hydrofluoric acid. The apparent differences in the etched surfaces are even greater than the photographs suggest when they are viewed through the microscope directly.

The previous semiannual report also had photographs of the etched Y-surfaces of LiNbO₃. Those photographs were even more illustrative than the present ones; however, they were obtained from a scanning electron microscope and, while informative, are not what is observed through a standard laboratory microscopy during routine wafer polarity determinations.

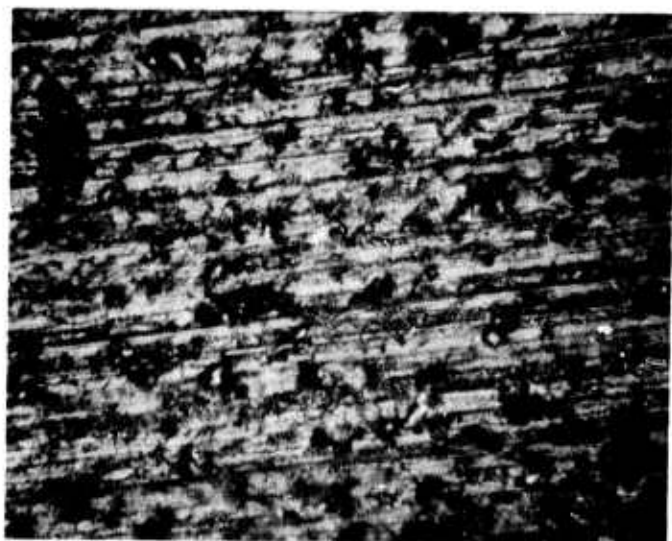
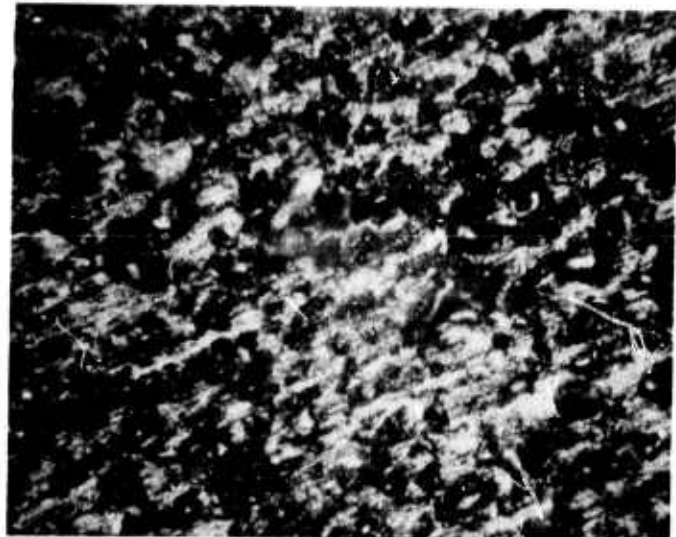


Figure 2 Y-Surfaces of a LiNbO₃ Wafer at ~ 500X.
Note the difference in appearance of the
+Y face (bottom photo) and the -Y face (top
photo) of the wafer after it was sawed from
a boule.

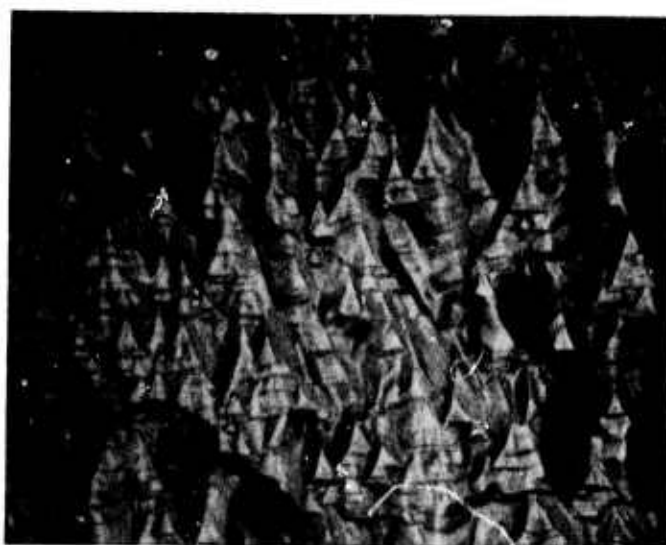


Figure 3 Y-Surfaces of a LiNbO₃ Wafer After Etching for About Two Hours in Boiling Concentrated HF. Top photograph shows the -Y face, bottom photograph the +Y face. Magnification $\sim 500X$.

Determination of the Z-axis polarity can also be made by hydrofluoric acid etching. In this case, however, standard laboratory microscopes are not adequate to see the high texture of the surface, and unlike that of the Y-faces, the appearance of the +Z-face tends to be dependent on the prior processing of the surface.

Figure 4 shows +Z and -Z faces of LiNbO_3 after etching in boiling concentrated hydrofluoric acid. The general appearance of the -Z face at $\sim 500X$ after etching for two hours is distinguishable. However, the depth of field of the microscope is not capable of bringing the entire picture into focus.

The two illustrations in Figure 4 of the +Z face show the difference prior processing makes in the appearance of the surface. The upper photograph shows the result after two hours of etching of the Z-flat of a (yz) LiNbO_3 plate as supplied by the vendor. That surface was then lapped in the X-direction only using 20 μm grit until it was completely roughened. It was then etched for another four hours to produce the appearance shown in the lower photograph. Polished +Z surfaces that are etched in boiling HF also have the appearance shown in the lower photograph of Figure 4.

SEM photographs of the $\pm Z$ surfaces illustrated in Figure 4 are shown in Figure 5.

From the current series of photographs and the two that appeared in the previous semiannual report, laboratory identification of the polarity of LiNbO_3 axes can readily be carried out. This should be of value not only in waveguide etching, but also in selecting a particular surface for wafer polishing.

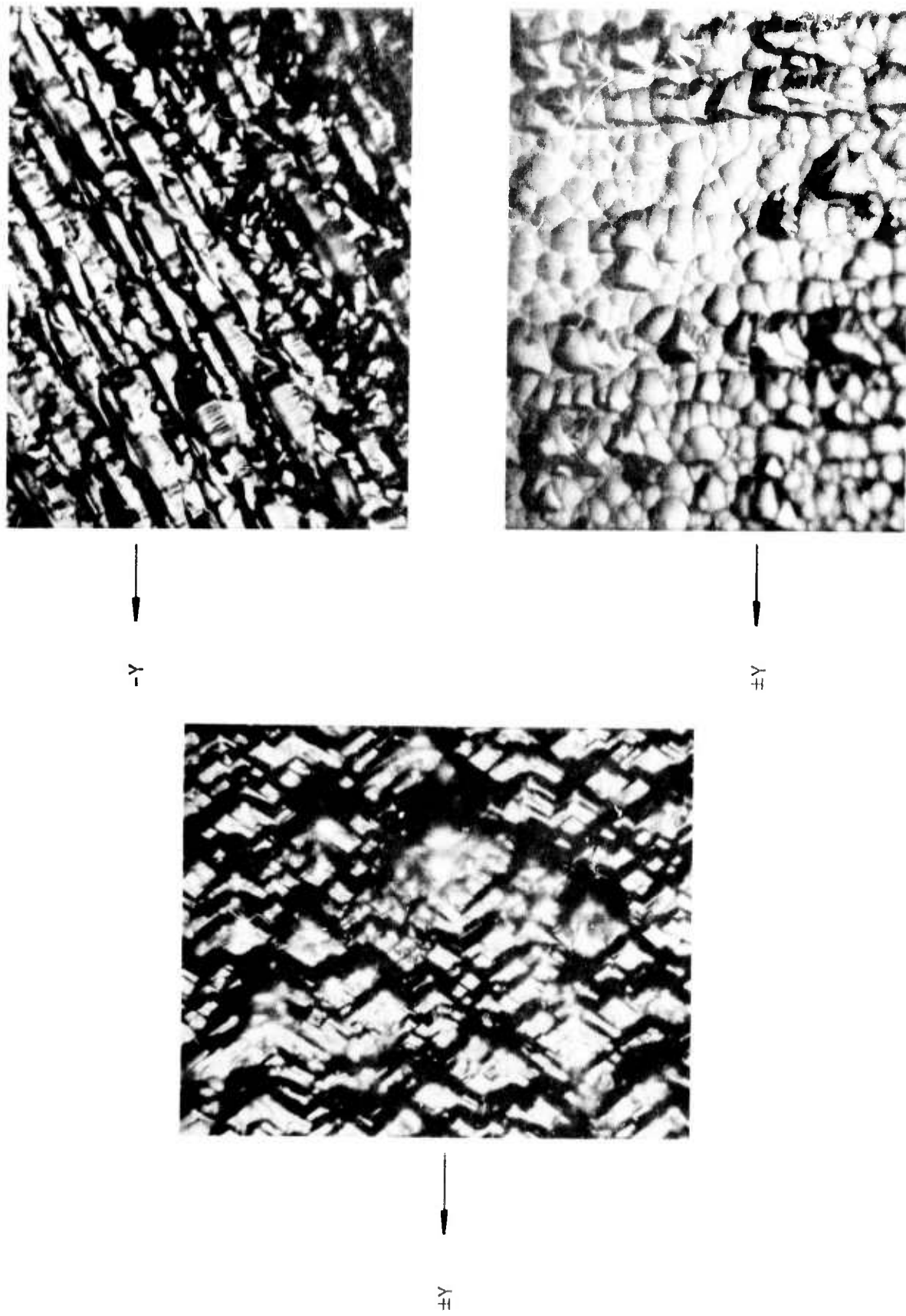


Figure 4 Z-Surfaces of LiNbO_3 After Etching in Boiling Concentrated HF. Magnification $\sim 500\times$. Left-hand photograph shows the $-Z$ face after two hours of etching. Upper right-hand photograph shows the $+Z$ flat on a wafer after two hours of etching. Bottom right-hand photograph shows the same $+Z$ surface after roughening in the $+X$ direction only and etching for another four hours.

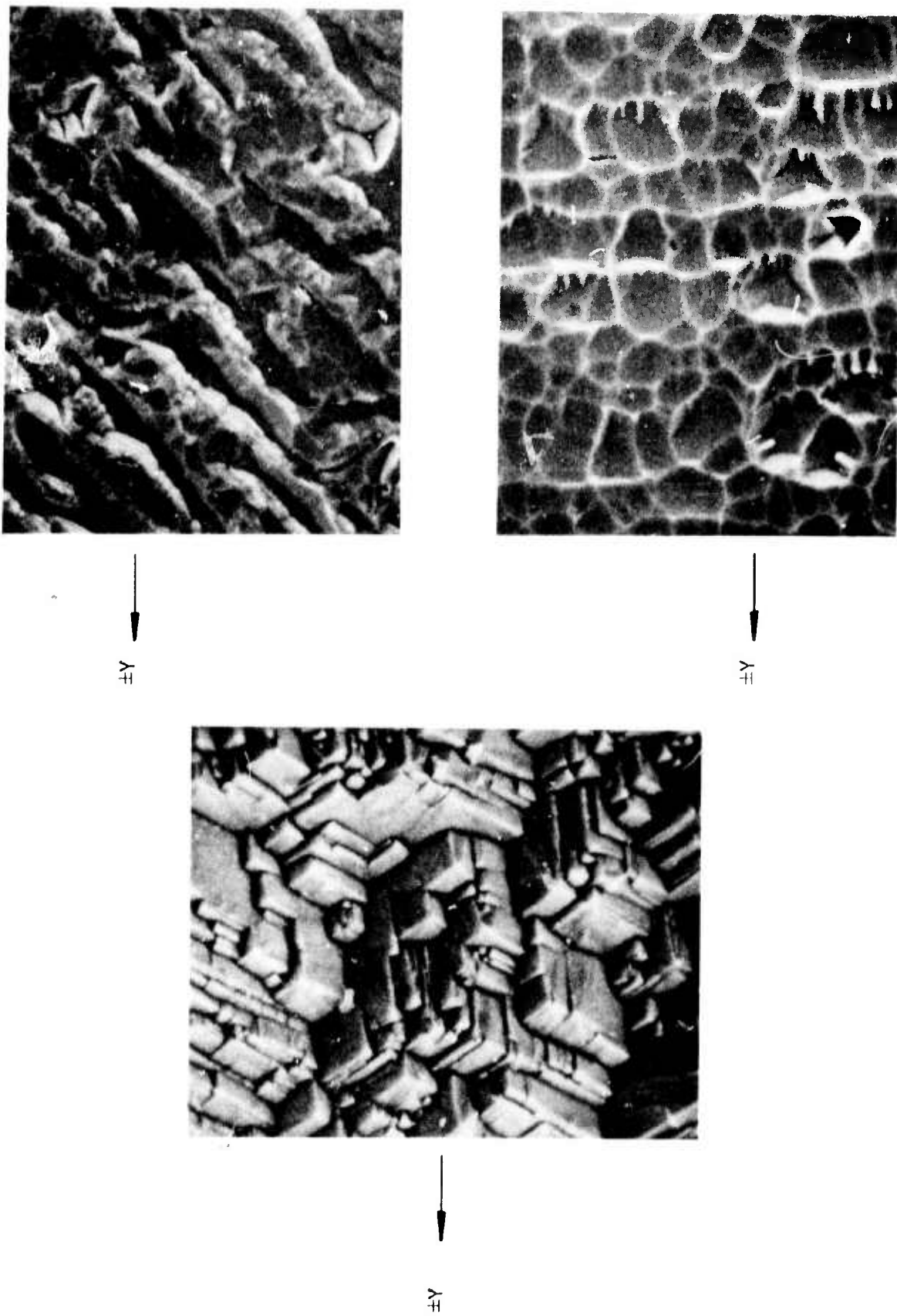


Figure 5 Scanning Electron Microscope Photographs of the Surfaces Shown and Described in Figure 4.

2. LiNbO_3 Etch Plane

The plane of LiNbO_3 which we have attempted to use as the lower face of the wedge waveguide is approximately $(20 \cdot \bar{3})$. As illustrated in Figure 6, it is parallel to the X-axis and down $\sim 26^\circ$ from the Y-plane. The 26° angle was determined empirically from multiple etching experiments. Calculations taking into account the unit cell dimensions, $a = 5.1483 \text{ \AA}$, $c = 13.863 \text{ \AA}$, and the 26° angle, give hexagonal lattice parameters of $(1.978 \ 0 \cdot \bar{3})$, which we have rounded to the values quoted above.

3. LiNbO_3 Waveguide Results

Our results on acoustic quality Y-cut LiNbO_3 have been uniformly discouraging. In general, we find that the crystals have very defective lattices, and the extent of their deviation from single-crystal is more than enough to prevent etching uniform waveguides. Higher quality LiNbO_3 has been obtained and is being processed, but waveguide results are not available at this time.

Figure 7 shows the same LiNbO_3 waveguide cross section photograph presented in the previous semiannual report. In that report we remarked on the single-faceted under-surface of the guide and its sharp apex while pointing out that these properties could not be maintained over an appreciable propagation distance.

Figure 8 shows how severe the waveguide uniformity problem can be. In this photograph the viewing angle is $\sim 10^\circ$ up from the plane of the wafer and the waveguides recede from view. Apex roughness is extreme and appears to be without characteristic form. That, however, is a consequence of the viewing angle. Under careful examination, the irregularities in the apex show a definite faceting. Also consider that relative to the apex of the guide, the back edge (upper surface) of the guide is quite uniform. Because of the quality of the back edge, it seems unlikely that irregular etch mask erosion is responsible for the waveguide nonuniformity.

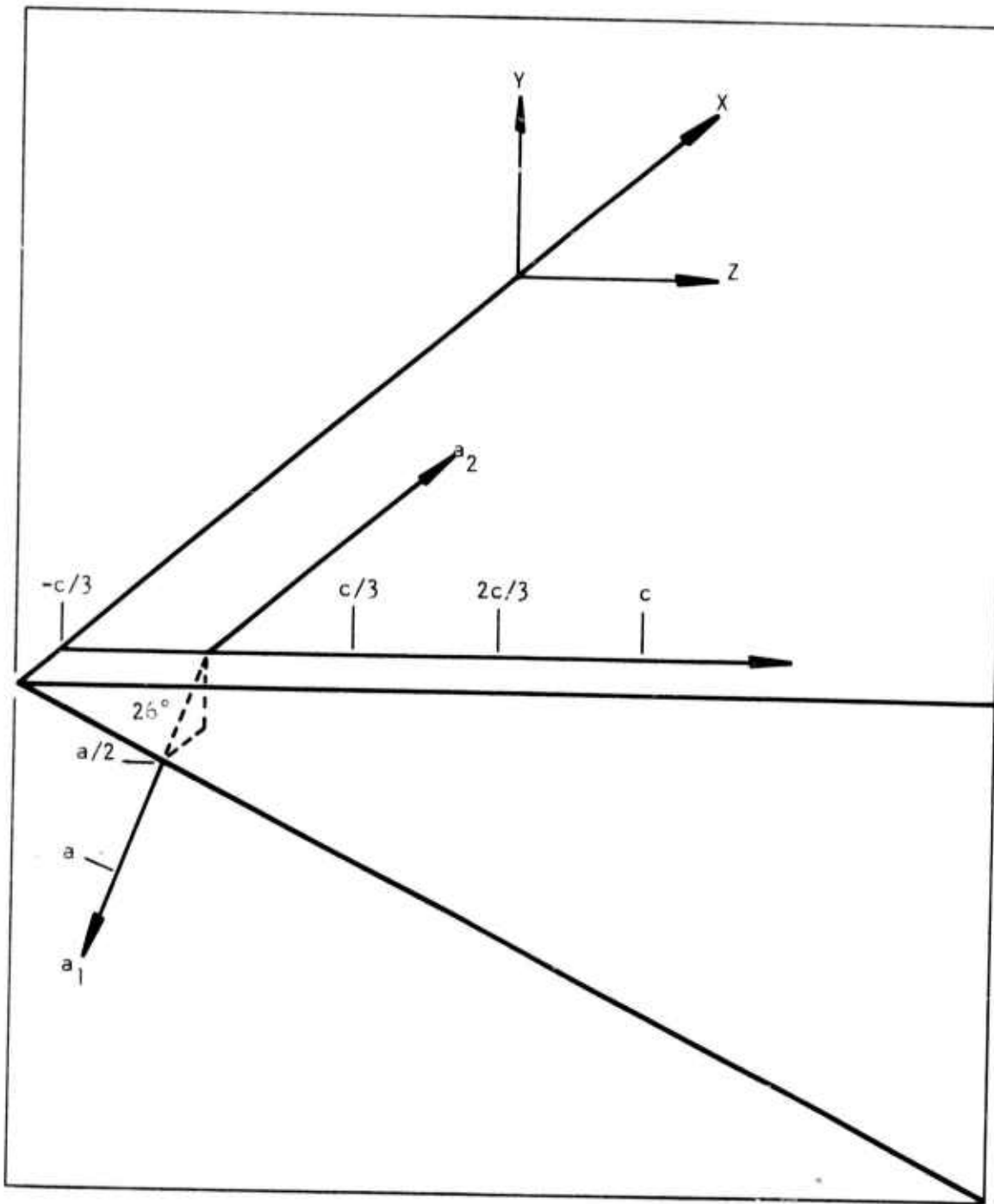


Figure 6 Schematic Representation of LiNbO_3 Waveguide
Showing Both Rectangular and Hexagonal Axes.
The lower surface of the waveguide is
approximately $(20 \cdot \bar{3})$.

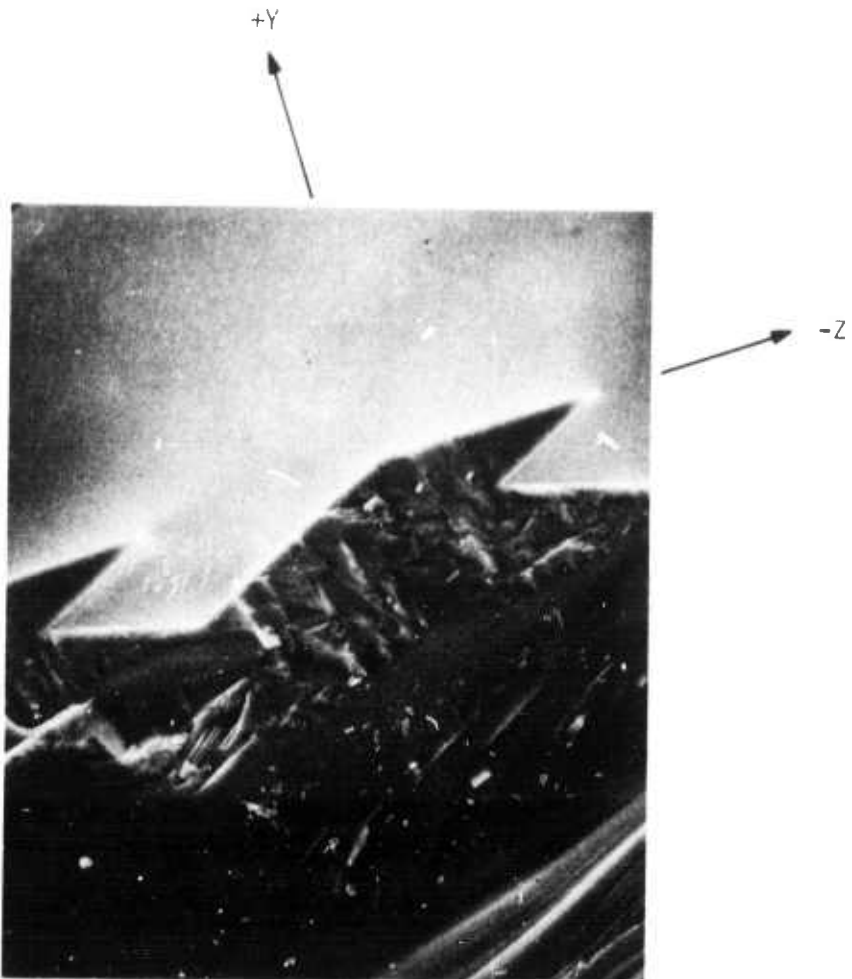


Figure 7 Etched LiNbO_3 Waveguides. Cross-sectional view at $\sim 800\times$.

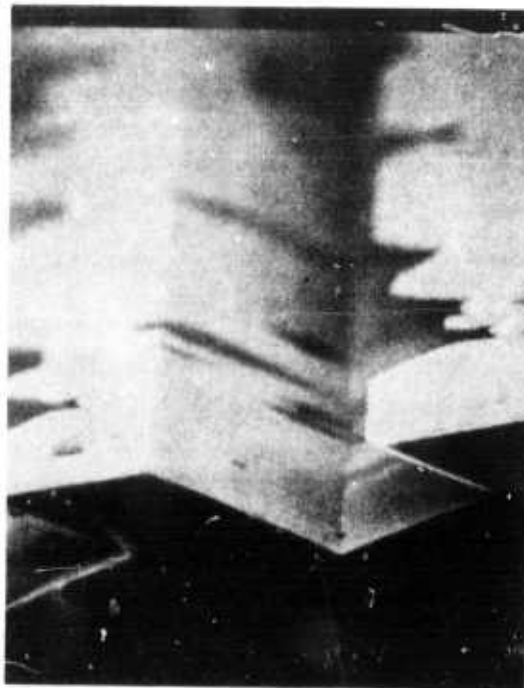
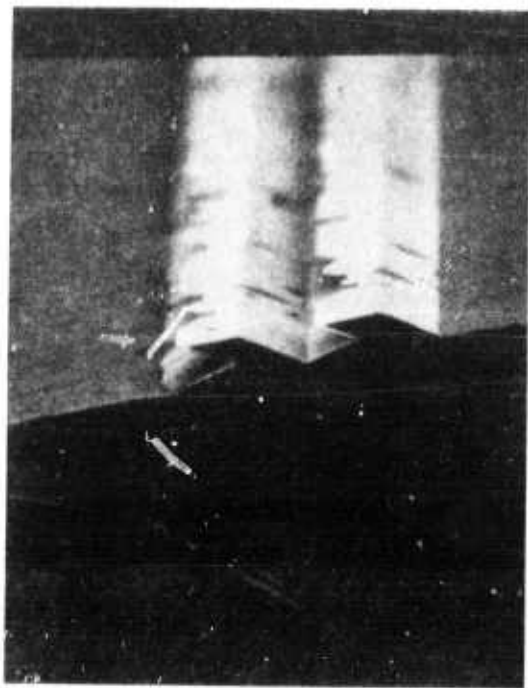


Figure 8 Two Etched LiNbO_3 Waveguides. Perspective views at $\sim 290\text{X}$ and 740X on the left- and right-hand sides, respectively.

The mosaic photograph in Figure 9 is a top view of the waveguides shown in Figure 8. Light regions in the illustration are the top surfaces of the waveguides, and dark regions have been etched down from the original wafer surface. The undercut edge is the lower side in all of the six waveguides. Now the faceting of the waveguide discontinuities is evident, and in a number of cases the problems can be traced from waveguide to adjacent waveguide. Again note that the top line of the waveguide upper surface (the edge not undercut) is relatively uniform.

The particular type of problem illustrated in Figure 9 is most likely due to inclusions in the material. If the wafer is tilted so that the viewing angle is as shown in the inset in Figure 10, then one sees faceted etch pits. These pits tend to correlate to the apex defects. The defect density varies from wafer to wafer, but in no case has this type of defect had a negligible density.

Polishing damage produces a different type of apex interruption. The photographs in Figure 11 illustrate what is thought to be damage due to subsurface microcracks induced during wafer grinding and polishing. Light regions in the photographs are the tops of the waveguides, and dark regions are the etched spaces between waveguides. The V-shaped indentations occur on the apex side of the waveguide and in some cases etch through to the other side of the waveguide. In the lower photograph some of the loci of defects move out of the field of waveguides into the unetched portion of the wafer. No visible crystal damage can be detected in the unetched crystal along the loci extrapolations or on the waveguide top surfaces, yet the damage is certainly present, as the etchant reveals. Note that the indentations in Figure 11 are V-shaped and point along the defect locus, whereas the faceted defects in Figure 9 have a definite Z-axis orientation.

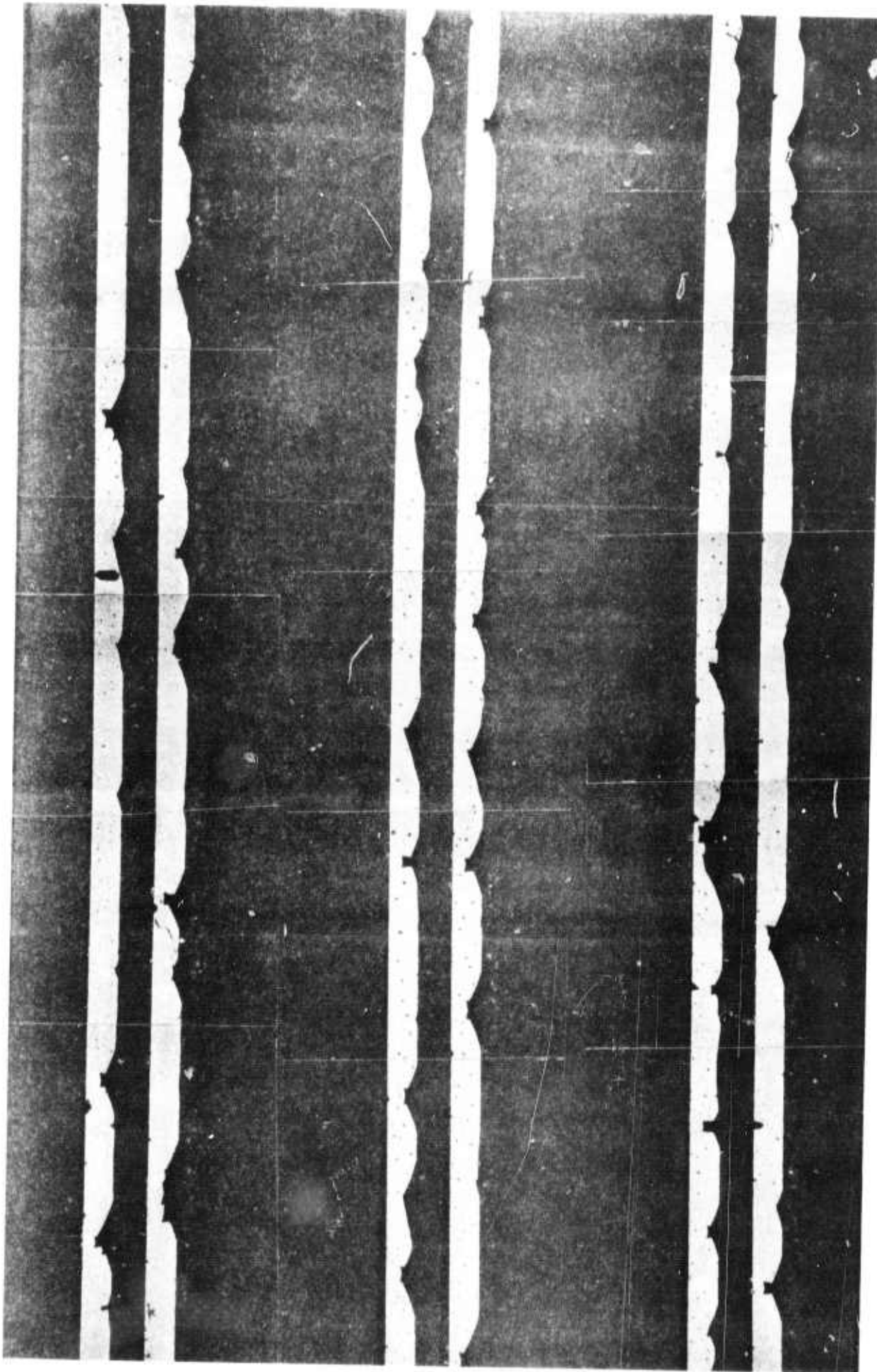


Figure 9 View at 100X Into the Y-Surface of Etched LiNbO_3 Waveguides.
The irregular lines are the undercut waveguide regions.

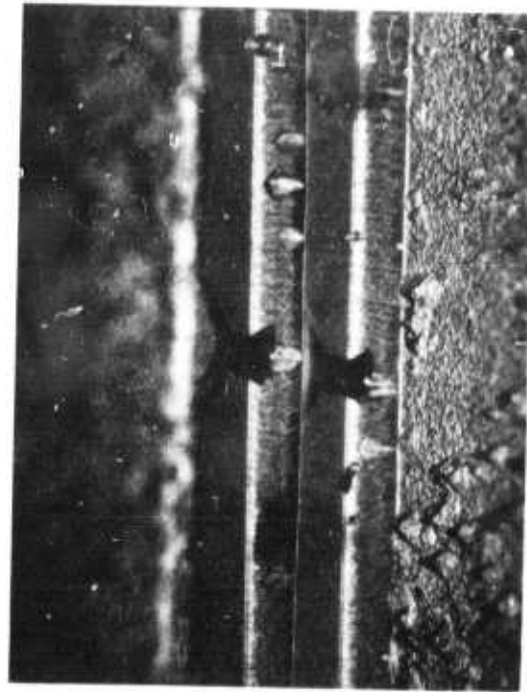
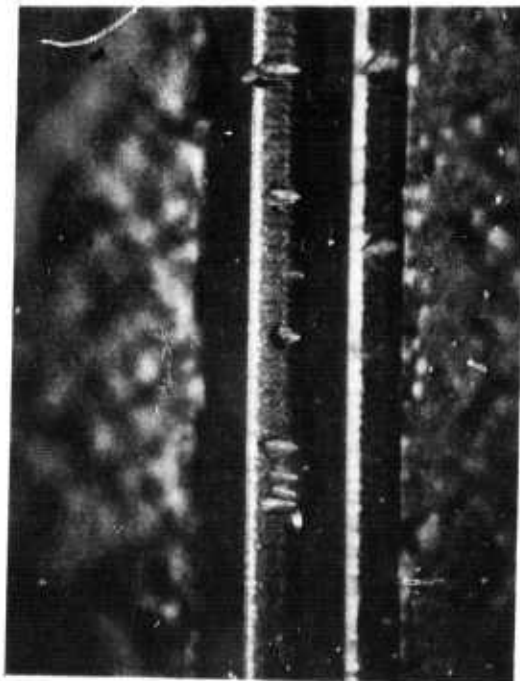
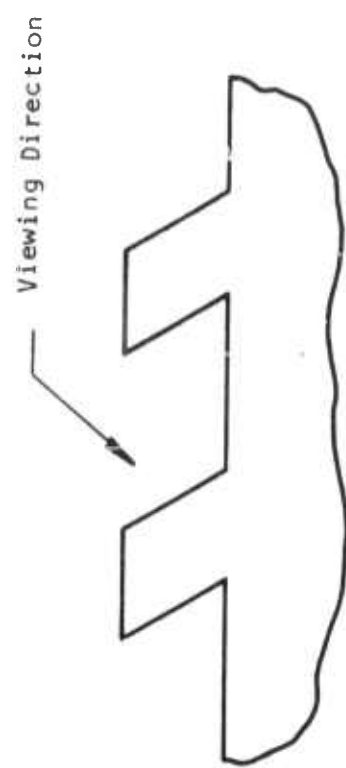


Figure 10 Etch Pits on the Side Wall of LiNbO_3 Waveguides, $\sim 100X$.

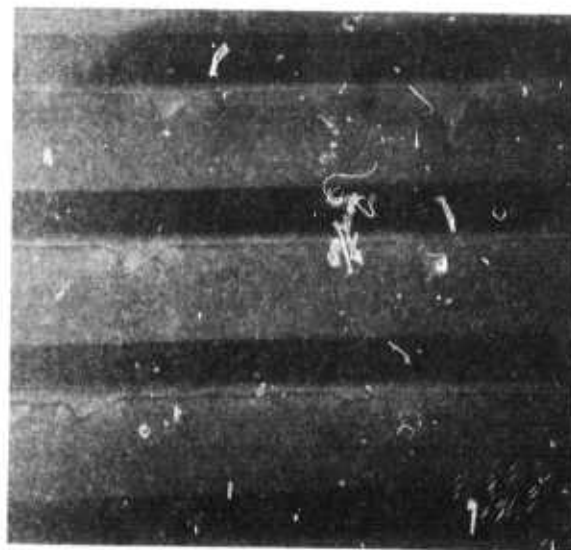
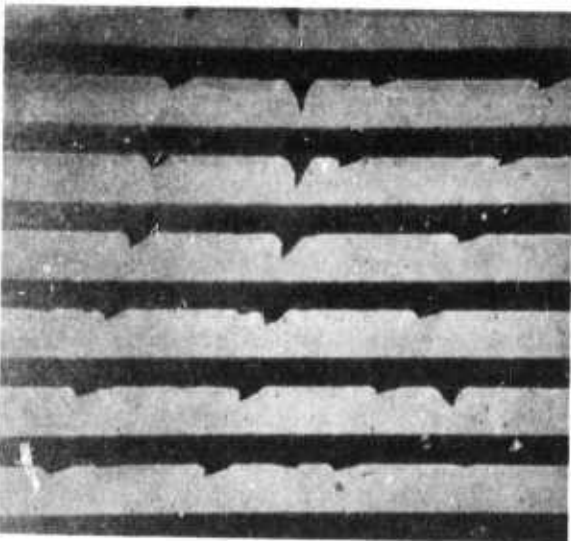


Figure 11 Polishing Damage in a Field of Etched LiNbO_3 Waveguides. Lower photograph at $\sim 100\times$. Upper left- and right-hand photographs at $\sim 250\times$ and $\sim 500\times$, respectively.

Another characteristic defect observed in the LiNbO₃ waveguides is shown in Figure 12. In this photograph the waveguides are the light regions, and the dark regions are the etched portion of the surface. The undercut edge is the lower edge in the photographs. Note that the waveguide apex has three faceted indentations. The apex line recedes from the etch mask edge at a shallow angle and then again runs approximately parallel to its original course before returning along another shallow-angled facet. The angle of these facets correlates well to a line structure that can be revealed in the Y-face of the wafer by etching with a 60:40 mixture by volume of H₂SO₄ and H₂O₂.

Figure 13 shows photographs of apex irregularities that correlate to a line structure on the Y-surface of the wafer. In this case the waveguide extends upward from the bottom of the photograph. Figures 13(a) through 13(c), which are a series of photographs of the same region at ~ 200X, ~ 500X, and ~ 1000X, show clearly that the apex defects indent from the line of the etch mask to specific planes of the crystal.

On the top surface of the waveguide one can see a line pattern that terminates at the corners of the indentations in the waveguide apex. This effect is most pronounced in Figure 13(d) (~ 1000X), where the defect was caused by either a scratch or an inclusion. What these lines are still has not been determined. We know that they are always present in the LiNbO₃ and that they correlate to demarcations in the etch characteristics of the crystal lattice. Also, they always have one of two characteristic appearances: they either are oriented at the shallow angle to the X-axis as shown in Figure 13, or they are exactly X-directed. Sometimes both orientations occur on the same wafer.

In an effort to determine if the line pattern was associated with volume effects within the crystal or was basically a short-range or surface effect, a 0.020 inch wafer of LiNbO₃ was polished on both +Y and -Y faces and etched in the H₂SO₄:H₂O₂ solution. After the line pattern was evident on the

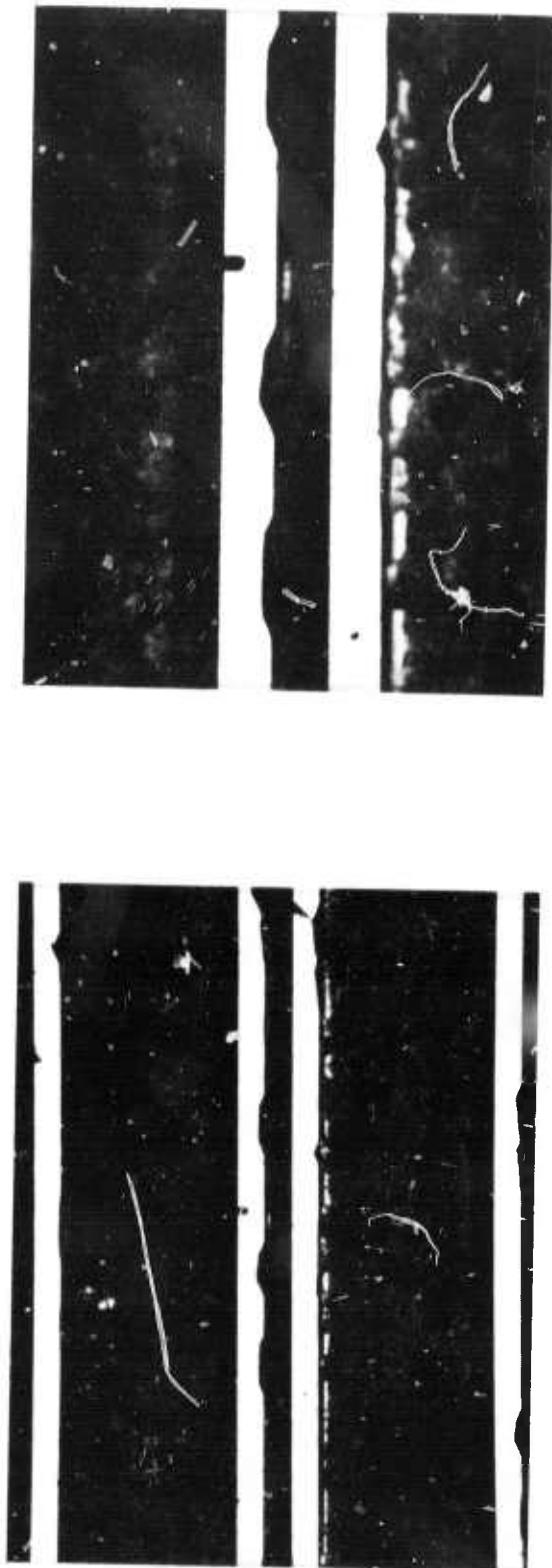


Figure 12 Etched LiNbO₃ Waveguides Showing Characteristic Indentations of Apex Line. Magnifications are ~50X and 100X in the left- and right-hand photographs, respectively.

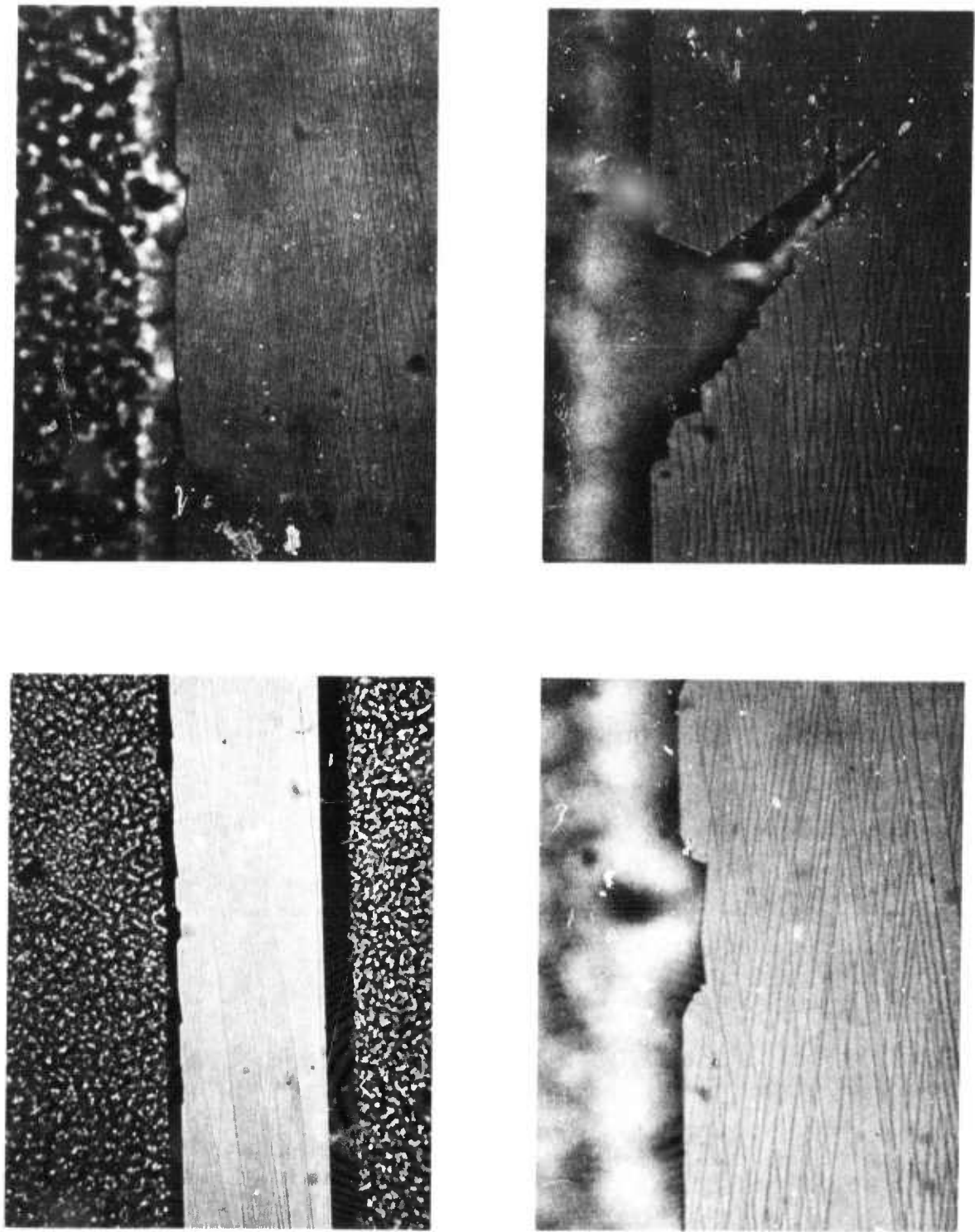


Figure 13 Correlation of Apex Defects With Y-Surface Line Structure.
Magnifications clockwise from upper left-hand corner are
 $\sim 200X$, $\sim 500X$, $\sim 1000X$, and $\sim 1000X$.

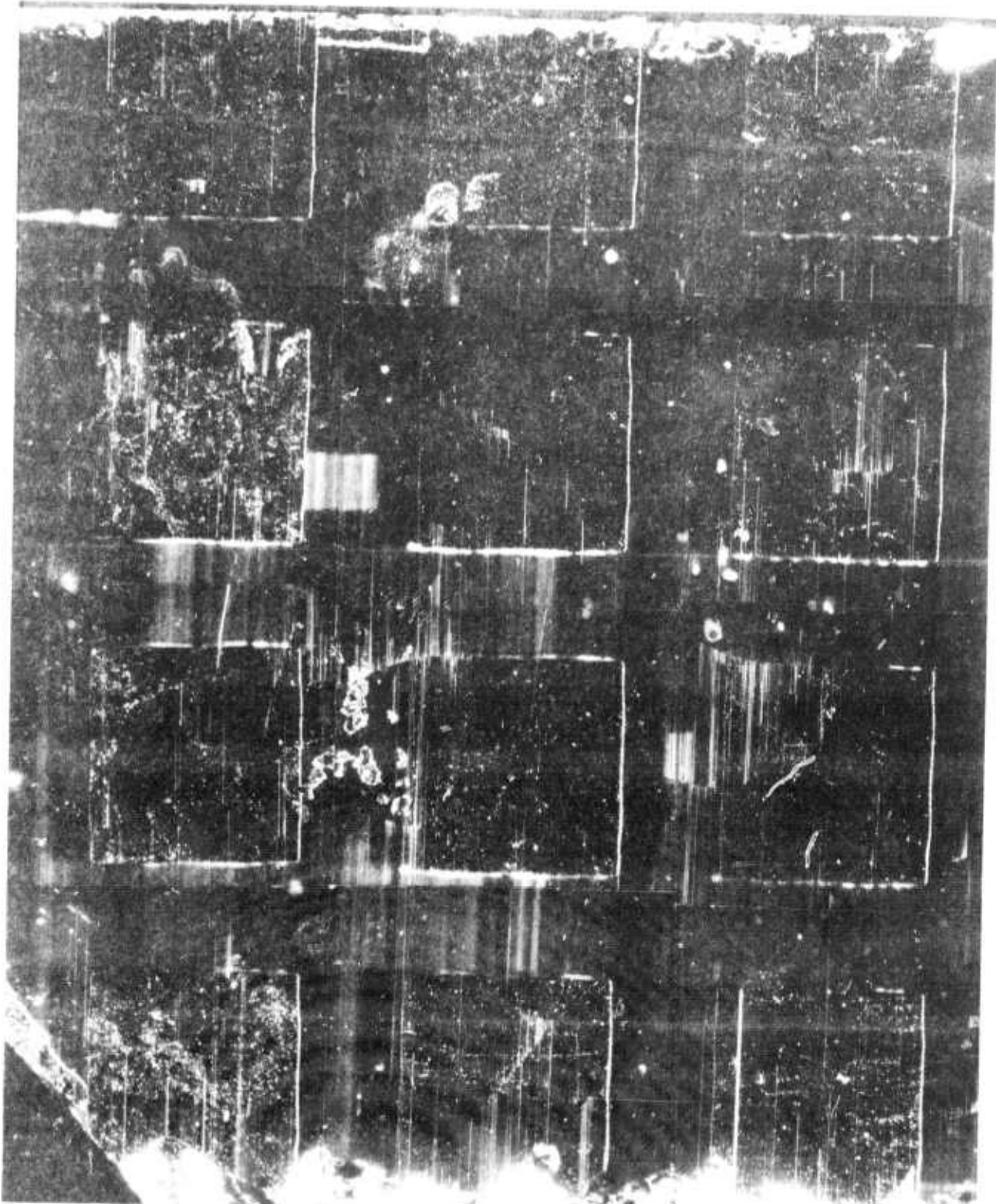


Figure 14 Y-Surface of LiNbO_3 Wafer. The 0.020 inch thick wafer was polished on both sides, etched to reveal the line structure shown, and had 0.080 inch \times 0.080 inch registration squares defined on the two surfaces.

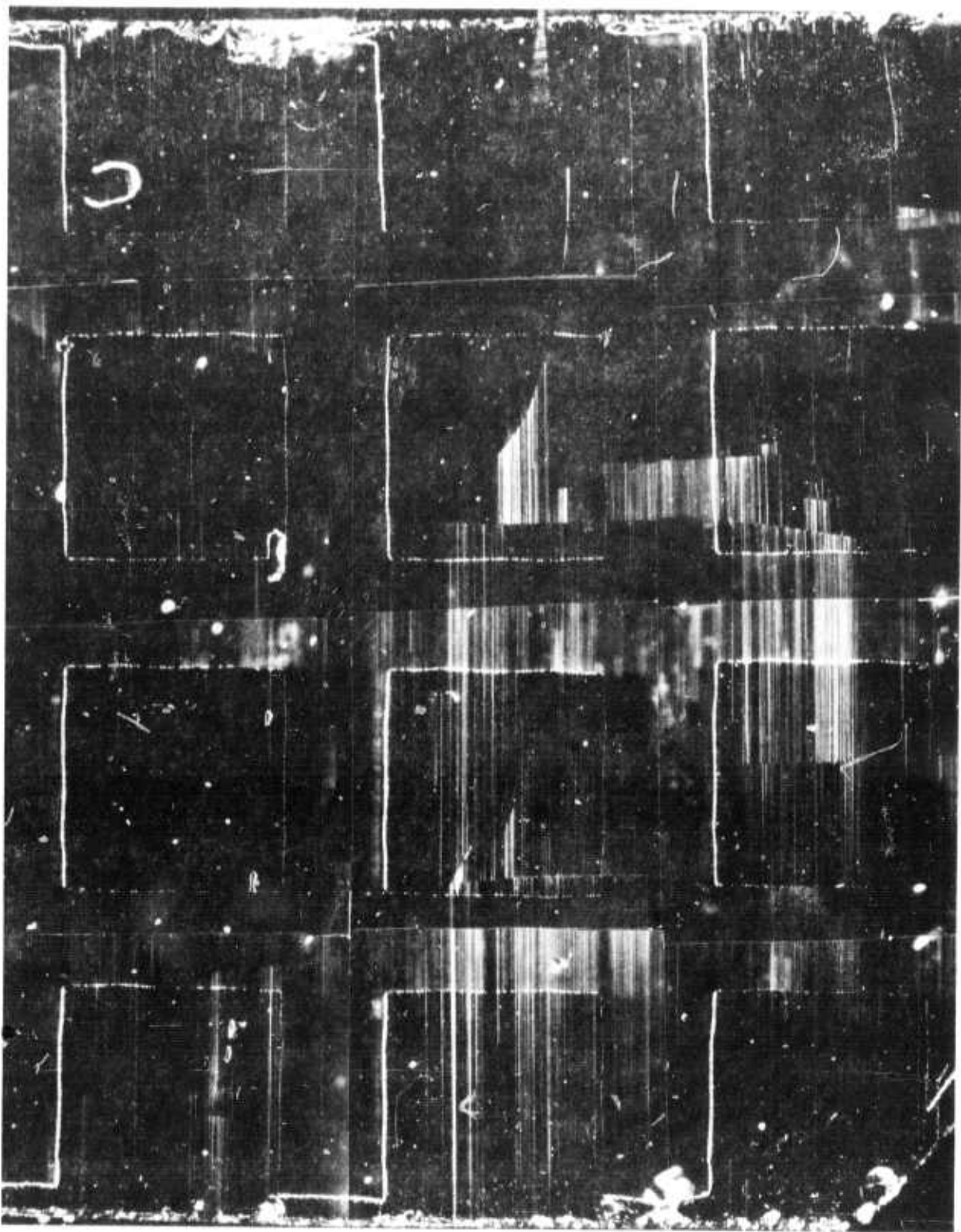


Figure 15 Y-Surface of LiNbO_3 Wafer. This is the surface opposite that shown in Figure 14.

surfaces, gold was evaporated on the two faces and then etched, leaving 0.080 inch x 0.080 inch squares on each face. The squares on the two faces were so arranged that the pattern on one face corresponded to a translation of the pattern from the other. With the two arrays of gold squares to serve as relative coordinates, one could examine the wafer to see if any effects could be traced through the 0.020 inch thick wafer.

Figures 14 and 15 illustrate the line structure on the two faces. The squares in the photographs are 0.080 inch by 0.080 inch, and illumination of the samples was from either the right- or the left-hand side at about 30° from the plane of the wafer. Taly-Step and SEM information indicates that the lines evident in the figures are on the order of 50 Å removed from the average plane of the wafer. When illuminated at normal incidence, the lines are virtually undetectable visually.

The features in Figures 14 and 15 can be divided into two classes, those that are in focus and those that are not. The in-focus features are on the top side of the wafer, while the cut-of-focus features are on the other side and are being seen through the LiNbO₃. The ability to see features through the wafer gives further registration of the two surfaces and allows one to look carefully for effects that track through the wafer. Even though there are a large number of features on the two surfaces, we cannot find one field of lines that truly tracks through the wafer. The effects either are localized volume effects with less than 0.010 inch range or are a consequence of surface preparation with less than 0.020 inch penetration. The question of surface preparation is still being examined.

C. Etching of α -Quartz

1. α -Quartz Crystal Defects

The previous semiannual report showed illustrations of highly uniform waveguides on ST-cut quartz. Those waveguides had defect-free propagation

distances on the order of 0.500 inch or more. Repeating these results and increasing the size of the waveguides from 0.001 inch to 0.003 inch has proved to be a challenge. First, the metallizations on the quartz are not withstanding the HF etch. Second, the longer etch times are revealing crystal defects in the quartz that we had not noticed previously. The defects were present in the earlier quartz devices, but they were sufficiently small that they were not noticed at that time.

The defects in quartz appear to be line defects that radiate out from the seed of the boule. The HF preferentially attacks these points on the unpolished side of the wafer and etches through to the waveguide side in a short time (\sim 30 minutes). If the etch times are long, in an effort to make large waveguides, the diameters of the line defects that permeate the crystal become large enough to disrupt the waveguides.

Figure 16 shows a sequence of four through-focus photographs of the line defects observed in quartz. The major light area is the upper surface of the crystal that was protected by the metals. The gray band is the over-hanging waveguide which extends downward. Magnification is \sim 100X, and moving from the upper left-hand corner clockwise, the focus is adjusted from the top of the wafer to the bottom. The line of the defects, which etched through from the back of the wafer to emerge at the top of the wafer under the chrome/gold, can be traced through the sequence of photographs. Figure 17 shows the same type of sequence at \sim 200X. Again, starting at the upper left-hand corner photograph and moving clockwise, the focus moves from the top of the crystal to the bottom.

2. Other Etchants and Etch Masks For Quartz

Because of the high rate of attack of HF on chrome/gold films on quartz, other etch masks and other etchants were examined. The other etch masks that were used with HF were sputtered molybdenum, sputtered molybdenum/gold, sputtered titanium/gold, and evaporated silicon. None of these films provided better protection than the sputtered chrome/gold films.

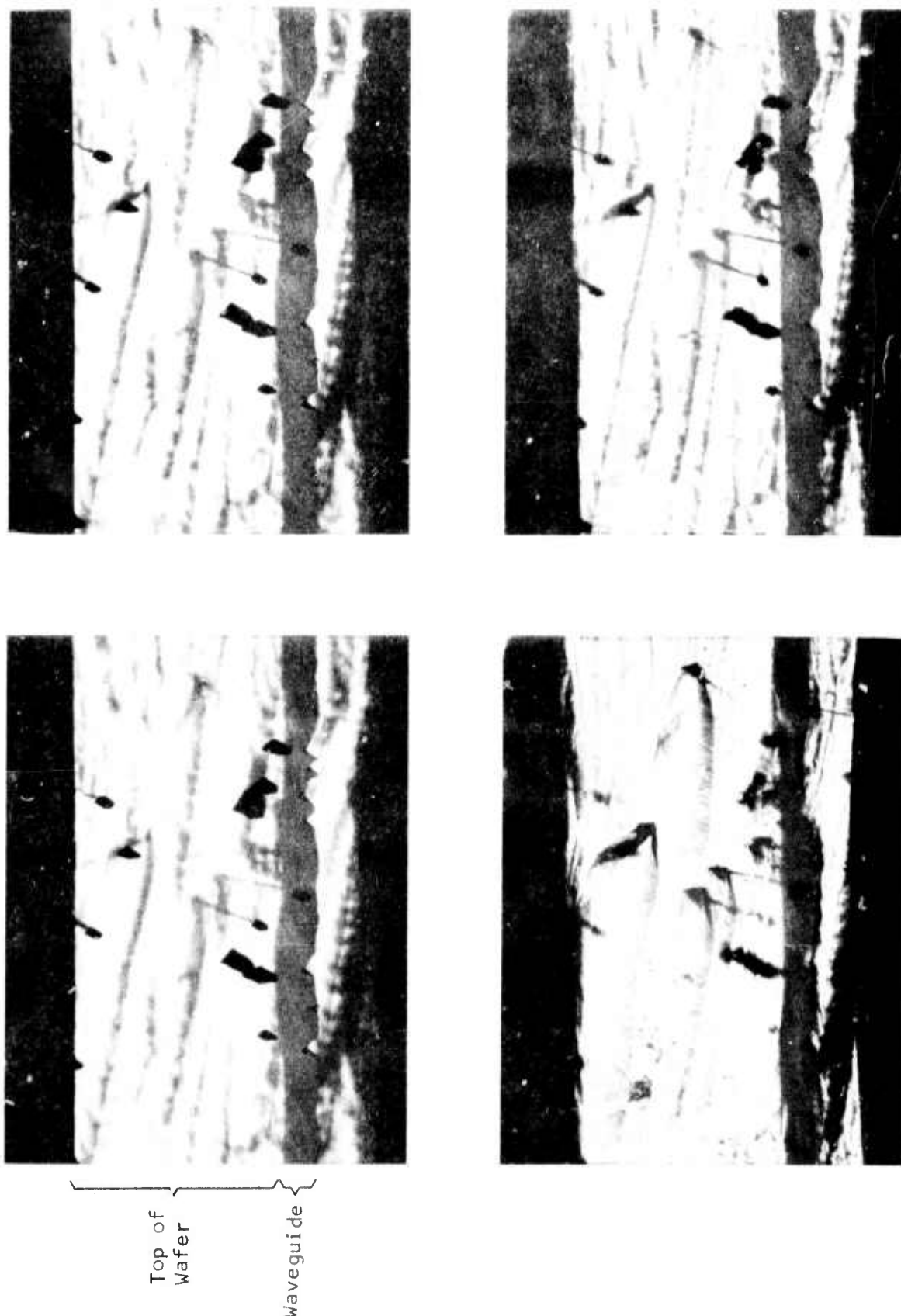


Figure 16 Waveguides on ST-Cut Quartz. Magnification is $\sim 100X$. The gray band below the major white region is the overhanging waveguide. Moving clockwise from the upper left-hand corner, the focus moves from the top of the crystal to the bottom. The course of defects through the crystal can be seen.

Figure 17 Waveguides on ST-Cut Quartz. A sequence of photographs like that in Figure 16, except at $\sim 200X$.



Two fluxes were also tried as etchants for quartz. The etch mask was sputtered chrome/gold in both cases. The first system was NaOH-KOH. A 50:50 Mol.% mixture of the two hydroxides liquefies at $\sim 170^{\circ}\text{C}$, and etching was carried out at just above the melting temperature. The substrates were ST-cut quartz patterned at various angles to see if orientation-dependent etching occurred anywhere on the plane.

We found that after only 12 minutes of etching, the chrome/gold film began to lift from the substrate. In addition, the etchant showed no orientational preferences, but instead etched essentially isotropically. The etch rate was extremely high, approximately 0.050 inch per hour.

Because Li_2CO_3 and K_2CO_3 , in theory, do not attack chrome, we tried a 50:50 by weight mixture of these two materials as an etchant. Unfortunately, this combination will not liquefy until the temperature reaches $\sim 500^{\circ}\text{C}$. Care must be taken in etching quartz at temperatures above 500°C because of the quartz phase change at 573°C . In the case of the carbonate mixture used here, however, the temperature problem is not a limiting factor, since the flux lifted the chrome/gold film from the substrate. We presume that impurities in the carbonates are responsible for etching the chrome. Once again, no preferential etching was detected.

D. Conclusion

In both quartz and LiNbO_3 crystal defects are a severe limitation to acceptable waveguide formation, and in LiNbO_3 they are the most important limitation. The defect density is sufficiently high that the longest propagation length between defects is measured in tens of mils. Erosion of the chrome/gold etch mask on LiNbO_3 is no longer considered a major problem, now that a more rigorous polishing standard has been adopted.

Quartz not only has crystal defects, but also presents an etch mask erosion problem that has not responded thus far to improved polishing procedures. Should the mask erosion problem be overcome, it is conceivable that very high frequency waveguides could be etched in quartz. The reason for the high frequency limitation is that long etch times reveal line defects in the quartz which disrupt the waveguides. However, it is not at all clear that waveguides limited to high frequencies ($\lambda \sim 10 \mu\text{m}$) would be workable, since relatively heroic efforts in transducer fabrication would be required to couple to the guide.

SECTION III
FUTURE WORK

During the final period of this work, weighting of apodized interdigital transducers on the apex of wedge-shaped waveguides will be examined. Both theoretical and experimental evaluation of transducer impedances will be performed as a function of transducer position on the waveguide. The normal mode theory will be applied to calculate coupling in the rapidly spatially varying field of the waveguide mode.

Experimental determination of transducer impedances will be carried out on Z-cut LiNbO₃ substrates. The substrates will be cut so that the lower surface of the waveguides is about 40° down from the Z-plane and propagation is along the X-axis. The apex points in the +Y direction. This orientation has very high coupling ($\Delta V/V = 0.0294$), and the electric potential of the fundamental mode is real, positive, relatively large, and slowly varying for the first four wavelengths away from the apex. The waveguides will be mechanically polished. Operation at about 2.0 MHz is intended.